Eur. Phys. J. D (2014) 68: 135
DOI: 10.1140/epjd/e2014-40818-y

THE EUROPEAN PHYSICAL JOURNAL D

Regular Article

Electron impact fragmentation of cytosine: partial ionization cross sections for positive fragments*

Peter J.M. van der Burgt[a]

Department of Experimental Physics, National University of Ireland Maynooth, Maynooth, Co. Kildare, Ireland

Received 20 December 2013 / Received in final form 20 March 2014
Published online 28 May 2014 –

Abstract. We have measured mass spectra for positive ions produced by low-energy electron impact on cytosine using a reflectron time-of-flight mass spectrometer. The electron impact energy has been varied from 0 to 100 eV in steps of 0.5 eV. Ion yield curves of most of the fragment ions have been determined by fitting groups of adjacent peaks in the mass spectra with sequences of normalized Gaussians. The ion yield curves have been normalized by comparing the sum of the ion yields to the average of calculated total ionization cross sections. Appearance energies of the fragment ions have been determined, showing that the fragments 68 u–84 u have appearance energies between 10 and 11 eV, whereas fragments of 55 u and lower mass all have appearance energies above 12 eV. Most of the ion yields of 55 u and smaller show multiple onsets. Several groups of fragments have ion yield curves with nearly the same shape, clearly indicating the relevance of tautomerization in the fragmentation of cytosine.

1 Introduction

Radiation induced processes in the DNA bases have been the focus of many studies in recent years, aiming at a better understanding of the fundamental reaction mechanisms leading to DNA strand breaks. When high-energy ionizing radiation passes through biological tissue, a large amount of secondary electrons are produced along the tracks of the ionizing radiation, mostly with energies below 30 eV, and these electrons are very effective in causing DNA strand breaks [1]. Even electrons with energies below the ionization energies of the DNA bases are capable of breaking bonds via dissociative electron attachment. For this reason, many recent studies have focused on electron collisions with DNA bases in the gas phase. Reviews of this field of molecular physics research can be found in review papers [2–5] and conference proceedings [6,7].

The purpose of this article is to present new results for the formation of positively charged fragments following low-energy electron impact to cytosine in the gas phase. Using computer-controlled data acquisition, we have measured mass spectra for 200 electron energies ranging from 0.5 to 100 eV, and from these we have extracted ion yield curves for most of the positive fragments. We have normalized these ion yield curves by comparison of the total ion yield to the total ionization cross section of cytosine obtained from theoretical calculations. These results provide new information about the appearance energies of the positive fragments, the fragmentation pathways initiated by electron impact, and the cross sections for production of these ions.

Cytosine has been the focus of a number of collisions studies involving electron, photon and ion impact. Rice et al. [8] present mass spectra obtained with 12 eV and 70 eV electron impact. Huels et al. [9] and Denifl et al. [10] have studied electron attachment to cytosine and present attachment cross sections for several negative ions in the range 0–14 eV. Shafranyosh et al. [11,12] have obtained total absolute cross sections for the production of positive and negative ions in electron collisions with cytosine molecules and present partial ionization cross sections at 78 eV. Other electron impact studies involve electron impact energy loss spectroscopy (Abouaf et al. [13], Johnson [14], and Michaud et al. [15]), differential elastic electron scattering (Maljkoviæ et al. [16]), and emission spectroscopy (Sphenik et al. [17]). Theoretical studies involving electron impact include R-matrix calculations by Dora et al. [18], calculations of elastic scattering cross sections and resonance energies by Tonzani and Greene [19], and calculations of total dissociative electron attachment cross sections by Aflatooni et al. [20].

A number of groups have looked at photofragmentation of cytosine, and have pointed out the relevance of the tautomeric forms of cytosine in the gas phase (see Fig. 1). We only list a few relevant recent references. Plekan et al. [21] present photofragmentation mass spectra of cytosine measured with noble gas resonance radiation at energies from 8.43 to 21.2 eV. Photofragmentation

* Contribution to the Topical Issue "Nano-scale Insights into Ion-beam Cancer Therapy", edited by Andrey V. Solov'yov, Nigel Mason, Paulo Limão-Vieira and Malgorzata Smialek-Telega.

[a] e-mail: peter.vanderburgt@nuim.ie

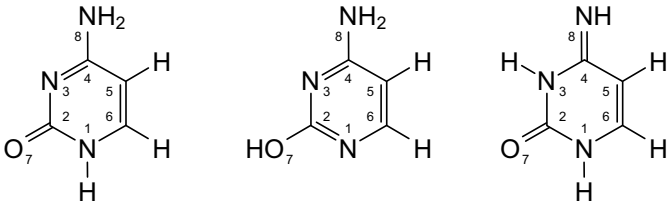

Fig. 1. Structure of the 1, 2a/b and 3a/b tautomers of the cytosine molecule.

with synchrotron radiation has been studied by Trofimov et al. [22], Kostko et al. [23] and Touboul et al. [24]. Nir et al. [25] have measured time-of-flight mass spectra of ions produced by resonant 2-photon ionization using lasers. Femtosecond pump-probe photoionization spectroscopy has been performed by Ho et al. [26], Kotur et al. [27] and Matsika et al. [28]. Scheidt et al. [29] have measured photodetachment of anion dipole-bound states of cytosine.

Only a few studies have been performed on ion impact of cytosine. Le Padellec et al. [30] present a mass spectrum for 100 keV proton impact on cytosine, and Tabet et al. [31] have measured mass spectra for 80 keV proton impact by direct ionization and by electron capture. Dal Capello et al. [32] present calculated differential and total cross sections for the direct ionization of cytosine by protons.

The present paper focuses on the production of positive ions by electron impact on isolated cytosine molecules in the gas phase. In the following sections we present a detailed discussion of our experimental set-up and data acquisition, and the methods used for analysis of the data. We then present the results, compare these with other research, in particular electron and photon impact mass spectrometry, and discuss possible reaction mechanisms.

2 Experiment

The experimental set-up consists of a resistively heated oven producing an effusive beam of cytosine molecules, a pulsed electron beam, and a reflectron time-of-flight mass spectrometer, housed in three inter-connected and differentially pumped vacuum chambers. More detailed descriptions of the set-up can be found in references [33,34]. The pulsed valve used in reference [33] for the generation of clusters has been replaced by the oven.

The molecular beam of cytosine is generated by heating the oven containing cytosine powder (99% purity from Sigma Aldrich) to a temperature of 240 °C. Comparison of mass spectra taken just before and after the data acquisition shows no sign of thermal decomposition. Molecules are effusing from a capillary (0.5 mm diameter and 4.5 mm length) in the oven and pass through a skimmer (1.2 mm diameter) into the collision chamber where they are collided with electrons.

The electron gun is pulsed at a rate of 8 kHz with a 1.0 μs pulse width. The energy resolution of the electron beam is about 0.8 eV FWHM. Positively charged fragments are extracted into the mass spectrometer 0.8 μs after the electron pulse. A delay generator is used to synchronise the pulsing of the electron gun, the ion extraction voltage, and the start of the multichannel scaler (FastComtec 7886S).

Data acquisition is controlled by LabVIEW code, which ramps the electron impact energy in 0.5 eV steps, acquires mass spectra as a function of electron impact energy, and adds each mass spectrum to the data already accumulated in the appropriate place in the full data set. The full data set consists of a two-dimensional array of ion yield as a function of time-of-flight and as a function of electron impact energy. After each scan of the electron impact energy, which takes about two hours, the full data set is written to a file. The data set used for this paper consists of 14 scans of the electron impact energy.

A number of tests have been performed to ensure that ionization cross sections and appearance energies could reliably be determined from the collected data. The optimization of the electron gun was done in pulsed mode by maximizing the current on the Faraday cup and ensuring that the current was independent of electron impact energy. In this way an electron beam was produced with a total current that is constant down to 15 eV and dropping to 60% at 8 eV. Tests have been done to ensure that the voltages used in the mass spectrometer were optimized simultaneously for the detection of ions of different masses (in the range 12–111 u). Two mass spectra were collected for an equal number of electron pulses at electron pulse rates of 8 kHz and 400 Hz, and were found to be identical apart from minor statistical fluctuations. By examining mass spectra obtained after successive scans, it has been verified that there were no undesired effects during the collection of the data presented in this paper.

3 Data analysis

The mass resolution of the mass spectrometer is $\Delta m/m = 0.005$ at 111 u, which is not high enough to fully separate adjacent peaks in the mass spectra. For this reason groups of adjacent peaks have been fitted using sequences of normalized Gaussians. Each group of peaks was extracted from the full dataset and imported in a LabVIEW program written to fit the peaks in the group for all electron impact energies in succession. As the electron impact energy reached values close to the appearances energies for the peaks, problems with convergence of the fits were encountered. For this reason most fits were repeated in a region of low electron energies using a reduced number of peaks and/or a fixed value of the peak width.

We have not been able to fully eliminate the presence of water in our vacuum system. 16–18 u fragments are observed in mass spectra regardless of the oven temperature. For this reason ion yield curves for these fragments are not presented. We see no indication of a cytosine-water dimer in the mass spectra, so the presence of water has had no effect on the data for cytosine.

The 17 u and 18 u ion yield curves obtained from the fitting procedure have been used for calibration of

the incident electron energy. The calibration was obtained by comparing our data with the recommended ionization cross sections for the production of H_2O^+ and OH^+ in Itikawa and Mason [35] (Tab. 11) in the range 10–40 eV. The estimated error in the calibration is ±0.2 eV.

Appearance energies for each of the fragments have been determined by fitting an onset function convoluted with a Gaussian (see Denifl et al. [36] and references therein). For a single onset at E, the formula used is:

$$P(E) = \int_{-\infty}^{\infty} f(\varepsilon) g(E-\varepsilon) d\varepsilon + b$$

with

$$f(\varepsilon) = 0 \qquad \text{if } \varepsilon \leqslant E_0$$
$$f(\varepsilon) = c(\varepsilon - E_0)^p \qquad \text{if } \varepsilon > E_0$$

and

$$g(\varepsilon) = \frac{1}{\sigma\sqrt{\pi}} \exp\left(-\varepsilon^2/\sigma^2\right).$$

In the case of two or three onsets, one or two extra terms were added to the function $f(\varepsilon)$. The fitting was implemented in LabVIEW.

4 Results and discussion

4.1 Total ionization cross section and normalization of the data

Assuming that the detection efficiency of the mass spectrometer is mass independent, and because all ion yield curves presented in this article have been generated from a single data set, all curves are on the same relative scale. The curves have been normalized by comparing the sum of the ion yield curves to the average of calculated total ionization cross sections at 70 eV.

We have obtained two curves for the total ionization cross section as a function of electron impact energy, shown in Figure 2. The first curve is the sum of all the ion yield curves obtained from the fitting procedure. This curve does not include the production of the 1 u, and the 16–18 u fragments because these fragments are largely due to the presence of water in our vacuum system. For this reason this curve slightly underestimates the total ionization cross section. The second curve is the sum of all the counts collected in the mass spectra as a function of electron impact, with the exclusion of 1 u, 16–18 u, and 32 u. This is a small overestimate of the total ionization cross section, because it contains background signals under and in between the cytosine peaks.

We have used a normalization factor of 3.36×10^{-25} for the first curve, which normalizes our data at 70 eV to the average of the theoretical cross sections presented in Figure 2. This provides good overall agreement with the shapes of the theoretical curves in the range 9–100 eV. We have used the same normalization factor for the second curve.

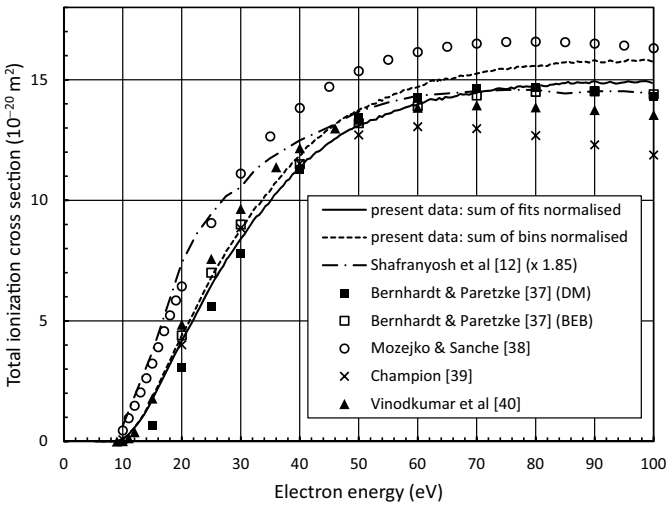

Fig. 2. Total ionization cross sections for electron impact on cytosine. The lines indicate experimental results; the symbols are theoretical results. For more details see text.

Figure 2 compares both curves with other experimental [12] and theoretical data [37–40]. To better compare the shapes of the curves, we have multiplied the data Shafranyosh et al. [12] by 1.85, such that it is also normalized to the average of the theoretical cross sections at 70 eV. Other calculations [41,42] are not shown in the graph; for comparisons see Figure 4 in Vinodkumar et al. [40].

Figure 2 shows that there is only a small difference between both curves, and the shapes of both curves are in good agreement with four of the theoretical calculations. The curve from Champion [39] drops more rapidly above 60 eV. The total ionization cross section of Shafranyosh et al. [12] rises more rapidly at low electron energies that any of the theories. In this respect our data is in better agreement with the theory than the data of Shafranyosh et al. [12].

4.2 Appearance energies

Figure 3 shows the appearance energies obtained for each of the thymine fragments. The errors have been obtained from the fitting of onsets in LabVIEW, and do not incorporate the error in the energy calibration. Four onsets above 30 eV are not shown in the graph: 12 u: 32.7±1.8 eV and 40.7±1.8 eV, 13 u: 34±3 eV, and 38 u: 33.0±0.7 eV. Apart from the appearance energy of the parent ion, to the best of our knowledge, no appearance energies of other fragment ions of cytosine have been published.

Our appearance energy for the parent ion is 8.4±0.5 V. This is in overall agreement with the other measurements and calculations of the ionization energies of cytosine listed in Table 1. Trofimov et al. [22], Kostko et al. [23] and Wolken et al. [46] have calculated vertical ionization energies for different cytosine tautomers. In cases where different calculation methods have been used and/or calculations have been done for different tautomers the lowest and highest values obtained are listed.

Table 1. Comparison of measurements and calculations of the appearance energy of the cytosine parent ion.

Reference	Experimental method	Measured ionization energy (eV)	Calculated vertical ionization energy (eV)
Present data	electron impact	8.4 ± 0.5	–
Trofimov et al. [22]	synchrotron radiation	8.89 ± 0.02	8.12–9.40
Kostko et al. [23]	synchrotron radiation	8.60 ± 0.05	8.86
Touboul et al. [24]	synchrotron radiation	8.66 ± 0.01	–
Hush and Cheung [43]	He I photo-el. spectr.	8.94 ± 0.03	8.81
Champeaux et al. [44]	–	–	8.6
Close and Øhman [45]	–	–	8.69–9.45
Wolken et al. [46]	–	–	8.68–9.02

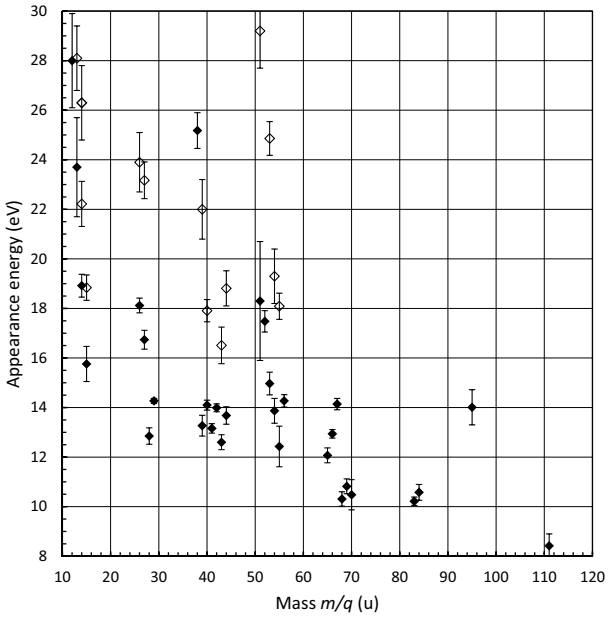

Fig. 3. Appearance energies for positive fragment ions of cytosine. For each fragment, the lowest onset is shown as a solid diamond, and higher onsets are shown as open diamonds. Four onsets above 30 eV are listed in the text.

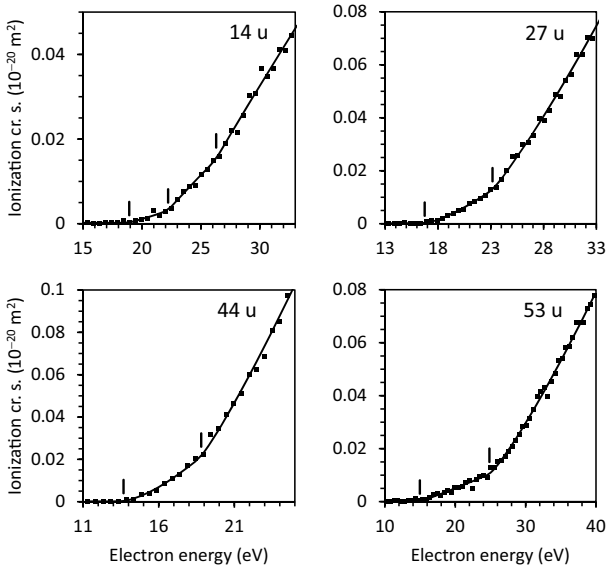

Fig. 4. Partial ionization cross sections of four of the smaller cytosine fragments. The appearance energies, second and third onsets, and fitted onset functions are also shown.

The second-lowest appearance energy is 10.22 ± 0.17 for 83 u. Appearance energies for 68 u, 69 u, 70 u and 84 u are all between 10 and 11 eV, whereas 97 u has an appearance energy of 14.0 ± 0.7 eV. All smaller fragments (56 u and lower) have appearance energies above 12 eV, indicating that all these fragments could be the result of successive fragmentations via 97 u, 83–84 u and 68–69 u.

Wolken et al. [46] have calculated dissociation energies of the cytosine cation radicals for several dissociations (see their Tab. 3). We have attempted to compare these with the difference in appearance energies of the fragment and the parent ion for the relevant fragments, but do not find any close agreement. Notably, the relative energies for the 68 u + 43 u and 69 u + 42 u dissociations calculated by Wolken et al. [46] are about 100 kJ/mol = 1.0 eV apart, whereas our appearance energies of 68 u and 69 u are 10.3 ± 0.3 eV and 10.8 ± 0.3 eV, respectively.

In many of the ion yield curves for fragments of 56 u and lower we observe second onsets. The ion yield curves of 12 u, 13 u and 14 u show clear indications of third onsets. Partial ionization cross sections for four fragments showing multiple onsets are shown in Figure 4. In all cases the difference in energy between the appearance energy and the second onset is 3 eV or higher. It is unlikely that these second onsets are linked to tautomerization, because the relative energies of the cytosine tautomers are less than 0.3 eV [47]. In several of the ion yield curves (28 u, 41 u, 68 u and 111 u) we do not find indications for a second onset, but the fitting with an onset function containing a single onset produced best values of the power p larger than 2, possibly indicating the presence of one or more additional onsets just above the appearance energy related to tautomerization.

4.3 Tautomerization and ion yield curves

Several authors have discussed the existence of cytosine tautomers. Figure 1 shows the structure of the cytosine tautomers. Trofimov et al. [22] have measured the photoelectron spectrum of cytosine at a source temperature of 190 °C, and conclude that this spectrum

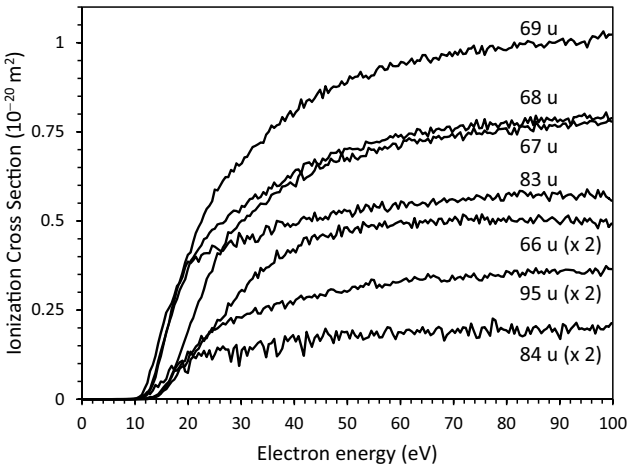

Fig. 5. Partial ionization cross sections of the most prominent fragments in the range 66–95 u. Above 35 eV the curves of 67 u, 68 u and 69 u have the same shapes, with yield ratios 67 u:68 u:69 u = 0.76:0.77:1. Above 40 eV, the yield ratio 83 u:84 u = 1:0.17.

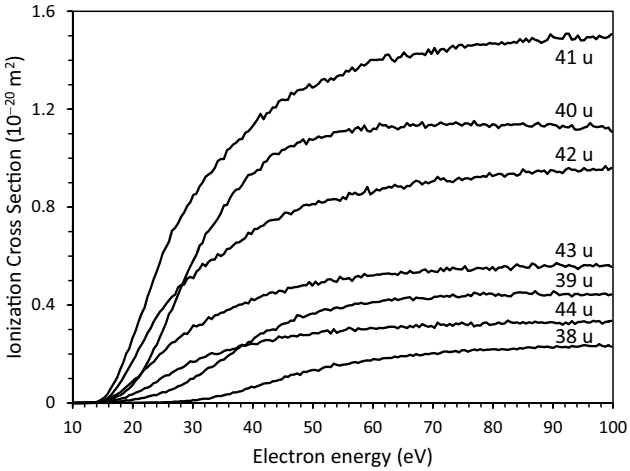

Fig. 6. Partial ionization cross sections of the 38–44 u fragments. Above 40 eV the curves of 41 u, 42 u, 43 u and 44 u have the same shapes, with yield ratios 41 u:42 u:43 u:44 u = 1:0.63:0.37:0.22.

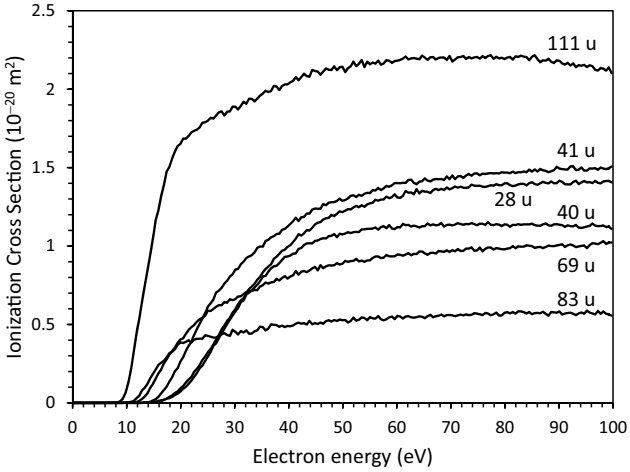

Fig. 7. Partial ionization cross sections of the 5 most abundant fragments of cytosine. Because of its low onset, the partial ionization cross section of 83 u is also shown.

can be attributed, largely, to the 2b tautomer. Populations of different cytosine tautomers based on calculations by various authors are presented in Table 1 of Kostko et al. [23]. Based on these results, we estimate that our oven (at 240 °C) produces the 1, 2a, 2b, 3a and 3b tautomers with relative populations of about 0.4, 0.5, 1.0, 0.1 and 0.02, respectively.

This also indicates that tautomerization preceding the dissociation may be significant in the sequential fragmentation of the radical cations. Atomic rearrangements prior to fragmentation have also been observed in other nucleobases (see eg. [48]). Comparison of the ion yield curves of the various groups of fragments clearly shows that several of the curves have very similar shapes, pointing towards the relevance of tautomerization.

The ion yield curves of 83 u and 84 u are shown in Figure 5. Apart from the parent ion, 83 u is the fragment with the lowest appearance energy. 84 u has an appearance energy that is only 0.36 eV higher. The 83 u and 84 u ion yield curves have very similar shapes: the 84 u/83 u yield ratio rises from 0.13 near threshold to 0.17 at 40 eV and is constant above that.

Of the peaks in the 65–70 u group, the ion yield curves of 67 u, 68 u and 69 u have the same shapes (see Fig. 5). Above 35 eV the yield ratios are 67 u:68 u:69 u = 0.76:0.77:1. From threshold to 35 eV the ion yield curves rise differently, and 67 u has a higher appearance energy than 68 u and 69 u. The ion yield curves of 65 u, 66 u and 70 u are clearly somewhat different in shape.

With the exception of 38 u, all fragments in the 38–44 u group have similar appearance energies. The partial ionization cross sections are presented in Figure 6. Despite differences in appearance energies and in the rise at low electron energies, above 40 eV the ion yield curves of 41 u, 42 u, 43 u and 44 u have the same shapes, with yield ratios 41 u:42 u:43 u:44 u = 1:0.63:0.37:0.22. The other ion yield curves in this group are clearly different in shape.

We do not notice any close similarities in the shapes of the ion yield curves of the 51–56 u group or of the fragments below 30 u.

4.4 Fragmentation processes

Partial ionization cross sections (normalized ion yield curves) for the five most abundant fragments of cytosine are presented in Figure 7. For comparison the partial ionization cross section of 83 u is also shown. Partial ionization cross sections for a selection of other fragments of cytosine are presented in Figures 5 and 6. A full set of partial ionization cross sections and appearance energies can be obtained from the author. A listing of possible allocations for each of the fragments can be found in Table 2 of Plekan et al. [21] and Table 3 of Tabet et al. [31].

Rice et al. [8] have proposed three distinct fragmentation pathways. The first pathway involves the expulsion of

the amino group, leading to the 95 u fragment. They suggest that subsequent loss of HCN could lead to formation of 68 u. We consider this unlikely, because the appearance energy of 95 u is higher than any of the appearance energies of the 65–70 u fragments and we do not find any indication of second onsets in the ion yield curves of this group. Based on the occurrence of second onsets in many of the ion yield curves of the smaller fragments, we propose that it is more likely that 95 u decays by breakage of two bonds in the ring, leading to fragments in group 3 (39–44 u) and group 4 (51–55 u).

The second fragmentation pathway is the formation of $C_3H_5N_3^+$ (83 u) by the loss of CO from the molecular ion. Further fragmentations, such as the expulsion of HCN, could then lead to fragments in the 51–56 u group. The other fragment in this group is 84 u. Tabet et al. [31] assume that 84 u is formed by loss of C_2H_2 and H, whereas Plekan et al. [21] attribute this fragment to N + CH loss with the breakage of 4 bonds. Based on the similarity of the ion yield curves of 83 u and 84 u, we propose a possible fragmentation involving the breakage the N1-C2 and C5-C6 bonds in the 1 and 2a/2b tautomers, leading to HCNH and HCN loss, respectively.

The third fragmentation pathway identified by previous authors [8,21] is the retro Diels-Alder reaction. This involves the expulsion of NCO or HNCO leading to 68 u and 69 u, or the loss of a hydrogen atom followed by HNCO leading to 67 u (which has a higher appearance energy). The similarity of these fragmentation processes is indicated by the similar shapes of the ion yield curves as discussed in Section 4.3.

The appearance energies of 67 u and 66 u are higher than those of 68–70 u, but are in the same range as the appearance energies of some of the smaller fragments (54–56 u, 39–44 u). 65 u is present in our mass spectra, with an appearance energy that is lower than those of 66 u and 67 u, but higher than those of 68–70 u. Denifl et al. [36] present dissociative electron attachment cross sections for the 67 u and 65 u negative ions.

The similarity in shape of the ion yield curves of 67–69 u and of 41–44 u strongly suggests that there is a common cause for this. One possible explanation is related to charge localization. Plekan et al. [21] have suggested that the ions in the group around 69 u are complementary to the ions in the group around 41 u, with the possibility of localization of the positive charge on either fragment. At low electron energies this is ruled out by the low appearance energies of the 68 u and 69 u fragments, but this may well be the case at higher electron energies. However, we note that the 70 u ion yield curve is somewhat different in shape compared to the 67–69 u curves, and also the shapes of the 67–69 u curves and the 41–44 u curves are different.

Another possible explanation is that the main successive fragmentation of the 67–69 u ions is to fragments of size 41–44 u. Rice et al. [8] have attributed the triplet of peaks at 40–42 u to HCN loss from 67–69 u. However, the 40 u ion yield curve is clearly different in shape than the 41–44 u curves. This explanation would therefore necessitate that the successive fragmentations be bracketed by 69 u to 44 u and by 67 u to 41 u, which could then only be the loss of C_2H and C_2H_2 from the 67–69 u ions.

The 51–56 u group contains a number of ions with relatively low abundance. We do not notice any close similarities in the shapes of these ion yield curves. 51 u, 52 u and 53 u have higher appearance energies than the other fragments in this group, indicating that these ions may be formed by hydrogen loss from 54 u, 55 u and 56 u. The third most abundant ion in this group is 52 u and a possible configuration of this fragment is $C_3H_2N^+$ [31], which could be formed by loss of a hydrogen atom from 53 u.

A number of fragments in this group could be formed directly by breakage of two bonds in the ring. 55 u and 56 u could be formed by the breakage of the C2-N3 and C5-C6 bonds. 54 u and 57 u, or alternatively 53 u and 58 u, could be formed by the breakage of the N3-C4 and N1-C6 bonds, but we note that 57 u is very weak in our mass spectra, and 58 u is almost absent.

Rice et al. [8] have suggested that 56 u may be formed by expulsion of HCN from 83 u. Other possibilities are HCNH loss leading to 55 u and HCCH loss leading to 57 u. The latter possibility is very unlikely given the very weak presence of 57 u in our mass spectra. Successive fragmentations via 95 u and 83 u could be possible for the formation of the ions in this group.

Various possible configurations of the fragments in the 39–44 u group have already been given by Plekan et al. [21] and Tabet et al. [31]. Fragments of different configuration in this mass range could be formed by breakage of two bonds in the ring and tautomerization could lead to fragments with one hydrogen atom more or less, but this would not explain the similarity in the shapes of the excitations functions for 41–44 u (see discussion of possible explanations above). The appearance energy of 38 u is substantially higher than the appearance energies of other fragments in this group. Possible allocations are $C_3H_2^+$ and C_2N^+, formed by the loss of one or more hydrogen atoms from heavier fragments in this group.

5 Conclusion

We have presented substantial new information about the electron-induced fragmentation of cytosine in the form of ion yield curves, partial ionization cross sections and appearance energies of the positively charged fragments. The appearance energies determined in the present work reduce the number of possible successive fragmentations leading to smaller fragments.

Notably the appearance energies of the 5 heavier fragments (68–84 u) are between 10 and 11 eV, whereas the appearance energies of the smaller fragments (67 u and lower) are all above 12 eV. 95 u has a high appearance energy of 14.0 eV, ruling out fragmentation of this ion by HCN loss. The fragments of 55 u and lower show second onsets, and 12–14 u show third onsets, indicating that multiple fragmentation pathways involving different successive fragmentations result to the formation of these

fragments. The appearance energies are in a few cases consistent with the loss of one or more hydrogen atoms from a heavier fragment.

Several groups of fragments (83–84 u, 67–69 u, and 41–44 u) have ion yield curves with very similar shapes above 35 or 40 eV, clearly indicating the relevance of tautomerization in the fragmentation of cytosine. The similarity in shape of the ion yield curves of 67–69 u on the one hand and of 41–44 u on the other hand is possibly due to breakage of the ring with charge localization on either fragment or due to a common fragmentation pathway for the 67–69 u ions.

For most of the smaller fragments different configurations and fragmentation pathways leading to their formation are still possible. More experimental and theoretical work is needed to further clarify the fragmentation pathways for the production of positive ions following electron impact on cytosine.

The author gratefully acknowledges financial support for scientific visits received from the Nano-IBCT project (COST Action MP1002) funded by the European Union.

References

1. B. Boudaïffa, P. Cloutier, D. Hunting, M.A. Huels, L. Sanche, Science **287**, 1658 (2000)
2. H. Hotop, M.-W. Ruf, M. Allan, I.I. Fabrikant, Adv. At. Mol. Opt. **49**, 85 (2003)
3. R. Balog, J. Langer, S. Gohlke, M. Stano, H. Abdoul-Carime, E. Illenberger, Int. J. Mass Spectrom. **233**, 267 (2004)
4. L. Sanche, Eur. Phys. J. D **35**, 367 (2005)
5. I. Baccarelli, I. Bald, F.A. Gianturco, E. Illenberger, J. Kopyra, Phys. Rep. **508**, 1 (2011)
6. B.A. Huber, C. Malot, A. Domaracka, Y.A. Gauduel, A. Solov'yov, J. Phys.: Conf. Ser. **373**, 011001 (2012)
7. *Radiation Damage in Biomolecular Systems*, edited by G. García Gómez-Tejedor, M.C. Fuss (Springer, 2012)
8. J.M. Rice, G.O. Dudek, M. Barber, J. Am. Chem. Soc. **87**, 4569 (1965)
9. M.A. Huels, I. Hahndorf, E. Illenberger, L. Sanche, J. Chem. Phys. **108**, 1309 (1998)
10. S. Denifl, S. Ptasińska, M. Probst, J. Hrušák, P. Scheier, T.D. Märk, J. Phys. Chem. A **108**, 6562 (2004)
11. M.I. Shafranyosh, M.I. Sukhoviya, L.L. Shimon, I.I. Shafranyosh, Tech. Phys. Lett. **31**, 1071 (2005)
12. I.I. Shafranyosh, M.I. Sukhoviya, M.I. Shafranyosh, J. Phys. B **39**, 4155 (2006)
13. R. Abouaf, J. Pommier, H. Dunet, Ph. Quan, Ph.-C. Nam, M.Th. Nguyen, J. Chem. Phys. **121**, 11668 (2004)
14. D.E. Johnson, Radiat. Res. **49**, 63 (1972)
15. M. Michaud, M. Bazin, L. Sanche, J. Chem. Phys. **137**, 115103 (2012)
16. J.B. Maljković, A.R. Milosavljević, D. Šević, B.P. Marinković, Publ. Astron. Obs. Belgrade **84**, 45 (2008)
17. O.B. Shpenik, N.M. Erdevdy, V.V. Zvenighorodsky, L.G. Romanova, J. Appl. Spectroscopy **80**, 43 (2013)
18. A. Dora, L. Bryjko, T. van Mourik, J. Tennyson, J. Phys. B **45**, 175203 (2012)
19. S. Tonzani, C.H. Greene, J. Chem. Phys. **124**, 054312 (2006)
20. K. Aflatooni, A.M. Scheer, P.D. Burrow, J. Chem. Phys. **125**, 054301 (2006)
21. O. Plekan, V. Feyer, R. Richter, M. Coreno, M. de Simone, K.C. Prince, Chem. Phys. **334**, 53 (2007)
22. A.B. Trofimov, J. Schirmer, V.B. Kobychev, A.W. Potts, D.M.P. Holland, L. Karlsson, J. Phys. B **39**, 305 (2006)
23. O. Kostko, K. Bravaya, A. Krylov, M. Ahmed, Phys. Chem. Chem. Phys. **12**, 2860 (2010)
24. D. Touboul, F. Gaie-Levrel, G.A. Garcia, L. Nahon, L. Poisson, M. Schwell, M. Hochlaf, J. Chem. Phys. **138**, 094203 (2013)
25. E. Nir, Ch. Plützer, K. Kleinermanns, M. de Vries, Eur. Phys. J. D **20**, 317 (2002)
26. J.-W. Ho, H.-Ch. Yen, W.-K. Chou, Ch.-N. Weng, L.-H. Cheng, H.-Q. Shi, Sz.-Hs. Lai, P.-Y. Cheng, J. Phys. Chem. A **115**, 8406 (2011)
27. M. Kotur, Th.C. Weinacht, C. Zhou, K.A. Kistler, Sp. Matsika, J. Chem. Phys. **134**, 184309 (2011)
28. Sp. Matsika, C. Zhou, M. Kotur, Th.C. Weinach, Faraday Discuss. **153**, 247 (2011)
29. J. Schiedt, R. Weinkauf, D.M. Neumark, E.W. Schlag, Chem. Phys. **239**, 511 (1998)
30. A. Le Padellec, P. Moretto-Capelle, M. Richard-Viard, J.P. Champeaux, P. Cafarelli, J. Phys.: Conf. Ser. **101**, 012007 (2008)
31. J. Tabet, S. Eden, S. Feil, H. Abdoul-Carime, B. Farizon, M. Farizon, S. Ouaskit, T.D. Märk, Int. J. Mass Spectrom. **292**, 53 (2010)
32. C. Dal Cappello, P.A. Hervieux, I. Charpentier, F. Ruiz-Lopez, Phys. Rev. A **78**, 042702 (2008)
33. G. Barrett, P.J.M. van der Burgt, J. Phys.: Conf. Ser. **101**, 012008 (2008)
34. P.J.M. van der Burgt, F. Mahon, G. Barrett, M. Gradziel, Eur. Phys. J. D, to be published
35. Y. Itikawa, N. Mason, J. Phys. Chem. Ref. Data **34**, 1 (2005)
36. S. Denifl, B. Sonnweber, G. Hanel, P. Scheier, T.D. Märk, Int. J. Mass Spectrom. **238**, 47 (2004)
37. Ph. Bernhardt, H.G. Paretzke, Int. J. Mass Spectrom. **223–224**, 599 (2003)
38. P. Możejko, L. Sanche, Radiat. Environ. Biophys. **42**, 201 (2003)
39. C. Champion, J. Chem. Phys. **138**, 184306 (2013)
40. M. Vinodkumar, Ch. Limbachiya, M. Barot, M. Swadia, A. Barot, Int. J. Mass Spectrom. **339–340**, 16 (2013)
41. W.M. Huo, C.E. Dateo, G.D. Fletcher, NASA Technical Report NAS-06-009 (2006)
42. A. Peudon, S. Edel, M. Terrissol, Radiat. Prot. Dosim. **122**, 128 (2006)
43. N.S. Hush, A.S. Cheung, Chem. Phys. Lett. **34**, 11 (1975)
44. J.-P. Champeaux, P. Çarçabal, M. Sence, P. Moretto-Capelle, P. Cafarelli, J. Phys. B **44**, 045205 (2011)
45. D.M. Close, K.T. Øhman, J. Phys. Chem. A **112**, 11207 (2008)
46. J.K. Wolken, Ch. Yao, F. Tureèek, M.J. Polceb, Ch. Wesdemiotis, Int. J. Mass Spectrom. **267**, 30 (2007)
47. G. Fogarasi, J. Mol. Struct. **413–414**, 271 (1997)
48. H.-W. Jochims, M. Schwell, H. Baumgärtel, S. Leach, Chem. Phys. **314**, 263 (2005)